Interlaboratory Comparison of Ultrasonic Backscatter Coefficient Measurements From 2 to 9 MHz

Keith A. Wear, PhD, Timothy A. Stiles, PhD, Gary R. Frank, Ernest L. Madsen, PhD, Francis Cheng, PhD, Ernest J. Feleppa, PhD, Christopher S. Hall, PhD, Beom Soo Kim, BS, Paul Lee, MS, William D. O'Brien, Jr, PhD, Michael L. Oelze, PhD, Balasundar I. Raju, PhD, K. Kirk Shung, PhD, Thaddeus A. Wilson, PhD, Jian R. Yuan, PhD

Objective. As are the attenuation coefficient and sound speed, the backscatter coefficient is a fundamental ultrasonic property that has been used to characterize many tissues. Unfortunately, there is currently far less standardization for the ultrasonic backscatter measurement than for the other two, as evidenced by a previous American Institute of Ultrasound in Medicine (AIUM)–sponsored interlaboratory comparison of ultrasonic backscatter, attenuation, and speed measurements (J Ultrasound Med 1999; 18:615–631). To explore reasons for these disparities, the AIUM Endowment for Education and Research recently supported this second interlaboratory comparison, which extends the upper limit of the frequency range from 7 to 9 MHz. ***Methods.*** Eleven laboratories were provided with standard test objects designed and manufactured at the University of Wisconsin (Madison, WI). Each laboratory was asked to perform ultrasonic measurements of sound speed, attenuation coefficients, and backscatter coefficients. Each laboratory was blinded to the values of the ultrasonic properties of the test objects at the time the measurements were performed. ***Results.*** Eight of the 11 laboratories submitted results. The range of variation of absolute magnitude of backscatter coefficient measurements was about 2 orders of magnitude. If the results of 1 outlier laboratory are excluded, then the range is reduced to about 1 order of magnitude. Agreement regarding frequency dependence of backscatter was better than reported in the previous interlaboratory comparison. For example, when scatterers were small compared with the ultrasonic wavelength, experimental frequency-dependent backscatter coefficient data obtained by the participating laboratories were usually consistent with the expected Rayleigh scattering behavior (proportional to frequency to the fourth power). ***Conclusions.*** Greater standardization of backscatter measurement methods is needed. Measurements of frequency dependence of backscatter are more consistent than measurements of absolute magnitude. ***Key words:*** backscatter; interlaboratory comparison; tissue characterization.

Abbreviations
AIUM, American Institute of Ultrasound in Medicine; MS, megasamples; RF, radio frequency; SNR, signal-to-noise ratio

Received September 21, 2004, from the Center for Devices and Radiological Health, US Food and Drug Administration, Rockville, Maryland USA (K.A.W.); University of Wisconsin, Madison, Wisconsin USA (T.A.S., G.R.F., E.L.M.); Boston Scientific, Fremont, California USA (F.C., J.R.Y.); Philips Research, Briarcliff Manor, New York USA (C.S.H., B.I.R.); Riverside Research Institute, New York, New York USA (E.J.F., P.L.); University of Southern California, Los Angeles, California (B.S.K., K.K.S.); University of Illinois at Urbana-Champaign, Urbana, Illinois USA (W.D.O., M.L.O.); and University of Tennessee, Memphis, Tennessee USA (T.A.W.). Revision requested November 18, 2004. Revised manuscript accepted for publication April 19. 2005.

The financial support of the American Institute of Ultrasound in Medicine's Endowment for Education and Research is gratefully acknowledged. The mention of commercial products, their sources, or their use in connection with material reported herein is not to be construed as either an actual or implied endorsement of such products by the Food and Drug Administration.

Address correspondence to Keith A. Wear, PhD, Center for Devices and Radiological Health, Food and Drug Administration, 12720 Twinbrook Pkwy, Rockville, MD 20852 USA.

E-mail: kaw@cdrh.fda.gov

Attenuation, sound speed, and the backscatter coefficient have been used to characterize many tissues, including blood, heart, eye, liver, kidney, prostate, and bone.[1–18] In 1998, the American Institute of Ultrasound in Medicine (AIUM) sponsored an interlaboratory comparison of methods for measure-

ment of attenuation, sound speed, and backscatter.[19] Ernest L. Madsen, PhD (University of Wisconsin, Madison, WI), oversaw the design, fabrication, and distribution of phantoms to 10 laboratories. Investigators performed measurements and submitted their results to Professor Madsen. The main conclusion of this effort was that there was broad agreement among the 10 laboratories regarding attenuation and sound speed measurements but considerable disparity regarding backscatter coefficient measurements.[19]

There are several factors that may contribute to the increased variance for backscatter measurements. First, attenuation and sound speed measurements are usually performed in the through-transmission mode. Because of the relatively low attenuation coefficients of biological tissues and tissue-mimicking media, the acquired radio frequency (RF) data (from which parameter estimates are derived) generally have a relatively high signal-to-noise ratio (SNR). Backscatter coefficient measurements, on the other hand, are performed in the pulse-echo mode. Because of the weak scattering properties of soft biological tissues and speckle noise, the SNR for backscattered RF data is comparatively low. A lower SNR contributes to increased variance of measurements. Second, there is a greater variety of measurement procedures and algorithms for assessment of the backscatter coefficient[20–29] than for the attenuation coefficient and sound speed. Third, the mathematical complexity of algorithms for computing the backscatter coefficient generally exceeds that for the attenuation coefficient and sound speed. Finally, attenuation and sound speed measurement techniques may be thoroughly tested by performing measurements on standard objects (eg, plastics, liquids, and rubbers) for which the true values are known. References for backscatter coefficients on such easily attainable test objects are comparatively rare (if they exist at all).

To further investigate disparities in backscatter coefficient measurements, the AIUM sponsored a second interlaboratory comparison study. The results of that study are reported herein.

Materials and Methods

Phantoms

As in the previous AIUM-sponsored interlaboratory comparison project,[19] Professor Madsen oversaw the design, fabrication, and distribution of test phantoms to participating laboratories. All materials were produced at the University of Wisconsin by methods reported previously.[30–32] Three batches of phantoms were produced, labeled A, B, and C. Each of the 11 participating laboratories received 3 phantoms, 1 from each batch. As in the previous interlaboratory comparison, each laboratory performed backscatter measurements (usually at multiple frequencies, depending on which transducers they had available) on each of the phantoms in their set. Because it is necessary to know the attenuation coefficient and sound speed to estimate the backscatter coefficient, participating laboratories measured and reported these parameters also.

The 3 types of tissue-mimicking materials were produced to provide variety in ultrasonic properties while still being representative of soft tissues. The properties of these materials were measured at the University of Wisconsin. Phantom A, which mimicked human liver, had an attenuation coefficient slope approximately equal to 0.4 $dB \cdot cm^{-1} \cdot MHz^{-1}$. Its frequency ($f$) dependence of backscatter was about $f^{2.1}$ over the frequency range of 2.5 to 5 MHz. Phantom B had an attenuation coefficient slope approximately equal to 0.7 $dB \cdot cm^{-1} \cdot MHz^{-1}$. Its frequency dependence was about $f^{3.2}$ over the frequency range of 2.5 to 5 MHz. Phantom C included millimeter-scale scatterers that sometimes occur in soft tissue. Its attenuation coefficient was in the range of values determined for in vitro human breast parenchyma reported by D'Astous and Foster.[33] Its backscatter coefficient (in the range of 2.5–5 MHz) was near the bottom of the range for in vitro human breast parenchyma. Its frequency dependence of backscatter was about $f^{0.55}$. (Average frequency dependences are $f^{1.3}$ for human breast parenchyma and $f^{0.8}$ for infiltrating duct carcinoma.[33])

Phantom properties are summarized in Table 1. The materials for phantoms A and B were produced according to the method of Madsen et al.[31] They were "macroscopically uniform," meaning that the only nonuniformity in either material resulted from the random positioning of microscopic glass bead scatterers. The scatterer number densities were about 5 scatterers/mm^3 (A) and 800 scatterers/mm^3 (B). The component materials (and relative amounts by weight) for the type A phantoms were agarose (3.5%),

n-propanol (3.4%), 75- to 90-μm-diameter glass beads (0.38%), bovine milk concentrated 3 times by reverse osmosis (24.5%), liquid Germall Plus preservative (International Specialty Products, Wayne, NJ) (1.88%), and 18-MΩ-cm deionized water (66.3%). The component materials for the type B phantoms were agarose (2.34%), *n*-propanol (2.92%), Potters 3000E glass beads (Potters Industries, Valley Forge, PA) (volume-weighted mean diameter of 26 μm with 90% having diameters <43 μm and 10% having diameters <9 μm) (1.87%), bovine milk concentrated 3 times by reverse osmosis (47.9%), liquid Germall Plus preservative (1.87%), and 18-MΩ-cm deionized water (43.1%).

The type C material consisted of gelatin-based spheres suspended in an oil-in-gelatin dispersion and was produced according to the method of Chin et al.[31,32,34] Before (random) suspension in the oil-in-gelatin dispersion, the spheres were sieved so that their diameters ranged between 0.6 and 1.7 mm. Fifty percent of the volume of the final type C material consisted of spheres, and 50% consisted of the oil-in-gelatin dispersion. The component materials (and relative amounts by weight) of the type C phantom spheres were gelatin (11.2%), *n*-propanol (4.06%), *p*-toluic acid preservative (0.073%), powdered graphite (16.3%), formalin (0.89%), and 18-MΩ-cm deionized water (67.4%). The mixture surrounding the spheres in the type C material consisted of gelatin (9.8%), *n*-propanol (5.07%), *p*-toluic acid preservative (0.063%), formalin (0.77%), 18-MΩ-cm deionized water (57.1%), detergent (0.93%), kerosene (12.2%), and safflower (14.0%).

The participating laboratories (except the University of Wisconsin) did not have knowledge of the phantom properties when they performed their measurements.

Table 1. Phantom Properties

Property	Phantom A	Phantom B	Phantom C
Scatterer	Glass beads	Glass beads	Gelatin-based spheres
Embedded in:	Agarose/*n*-propanol/milk/H_2O	Agarose/*n*-propanol/milk/H_2O	Oil-in-gelatin dispersion
Scatterer diameter	75–90 μm	9–43 μm	0.6–1.7 mm
Concentration	5/mm^3 (0.035% by volume)	800/mm^3 (0.7% by volume)	50% by volume

Phantom Boundary Layer Transmission

Each phantom was wrapped in a thin layer of plastic film (Saran Wrap; Dow Chemical, Midland, MI). It was necessary to know the ultrasonic transmission properties of the Saran layer to make accurate estimates of attenuation and backscatter coefficients. Experimental measurements and numerical computations of ultrasonic transmission coefficients of the Saran layers were conducted at the University of Wisconsin. A table of amplitude transmission coefficients for each sample was provided to each participating laboratory. The values presented in these tables were based on considering each of the 2 Saran Wrap layers separately and multiplying the entrance transmission coefficient (from water through Saran Wrap and into the sample) by the exit transmission coefficient (from the sample through Saran Wrap and into water). In general, the entrance and exit transmission coefficients are different from each other.

Ignoring attenuation in any of the media, the complex transmission coefficient for perpendicular incidence through a single, thin layer of Saran is given by

$$(1)\quad \frac{2Z_f}{(Z_i+Z_f)\cos(k_{saran}\,l)+j\,(Z_{saran}+\frac{Z_iZ_f}{Z_{saran}})\sin(k_{saran}\,l)},$$

where $j=\sqrt{-1}$; Z_i is the acoustic impedance of the incident material; Z_{saran} is the acoustic impedance of the Saran layer; Z_f is the acoustic material of the final material; k_{saran} is the wave number in the layer; and l is the thickness of the layer.[35] If attenuation in the 3 media is considered, the acoustic impedances and wave number become complex. However, except for sample materials with unrealistically large attenuation coefficients, the dominant contribution is due to the complex wave number in the argument of the trigonometric functions. Therefore, attenuation effects can be included in Equation 1 by setting

$$(2)\quad k_{saran}=\frac{2\pi f}{c_{saran}}-j\alpha(f),$$

where c_{saran} is the speed of sound, and α is the frequency-dependent attenuation coefficient of Saran Wrap.

In both through-transmission and pulse-echo experiments, the sound beam first enters from water through the Saran layer and into the sam-

ple and then exits from the sample through the Saran layer and into water. Therefore, the total effect on the magnitude of the ultrasound signal is equal to the product of the absolute value of Equation 1 with $Z_i = Z_{water}$ and $Z_f = Z_{sample}$ and the absolute value of Equation 1 with $Z_i = Z_{sample}$ and $Z_f = Z_{water}$, namely,

$$abs\left(\frac{2Z_{sample}}{(Z_{water}+Z_{sample})\cos\left(\left(\frac{2\pi f}{c_{saran}}-j\alpha(f)\right)l\right)+j\left(Z_{saran}+\frac{Z_{water}Z_{sample}}{Z_{saran}}\right)\sin\left(\left(\frac{2\pi f}{c_{saran}}-j\alpha(f)\right)l\right)}\right)\times$$
$$abs\left(\frac{2Z_{water}}{(Z_{sample}+Z_{water})\cos\left(\left(\frac{2\pi f}{c_{saran}}-j\alpha(f)\right)l\right)+j\left(Z_{saran}+\frac{Z_{sample}Z_{water}}{Z_{saran}}\right)\sin\left(\left(\frac{2\pi f}{c_{saran}}-j\ (f)\right)l\right)}\right), \quad (3)$$

where Z_{water}, Z_{sample}, and Z_{saran} are the acoustic impedances of water, the sample, and Saran Wrap, respectively; c_{saran} is the speed of sound in Saran Wrap; f is the frequency (in Hertz); $\alpha(f)$ is the frequency-dependent attenuation coefficient of Saran Wrap (in nepers per meter); and l is the thickness of the Saran Wrap. Note that all variables in this expression are real numbers.

The thickness of the Saran Wrap used for these samples was measured with a micrometer to measure the thickness of 32 layers of the material and found to be 25.1 ± 0.5 μm (mean ± SD). The acoustic impedance of a material is equal to its density multiplied by its speed of sound. The density of Saran Wrap was measured by computing the ratio of the mass and volume of a large sheet of Saran Wrap and found to be 1.69 ± 0.02 g/cm^3.

To quantify the speed of sound and attenuation coefficient of Saran Wrap, the amplitude transmission coefficient of a single layer of Saran Wrap in water was measured by a narrow-band technique. The experimental setup consisted of a water tank, a Wavetek (now Fluke Corporation, Everett, WA) model 81 function generator, an Amplifier Research (Souderton, PA) model 75A250 RF power amplifier, a LeCroy (Chestnut Ridge, NY) model 9410 digital storage oscilloscope, and several pairs of unfocused transducers (Panametrics, Waltham, MA; and Aerotech, Lewistown, PA) with various center frequencies. The function generator created a low-amplitude voltage signal of 30 cycles at a specific frequency, which was amplified and sent to a transmitting transducer. The signal detected by the receiving transducer was displayed directly on the oscilloscope, which was triggered with a pulse from the function generator that was synchronous with the start of the output voltage pulse. Received waveforms with and without the Saran film in the ultrasound path were acquired. Ten measurements in 1-MHz steps were made between 1 and 10 MHz with the use of several pairs of transducers with common nominal center frequencies. Thirty-one measurements were conducted between 15 and 50 MHz with 1 pair of 30-MHz broadband transducers. Table 2 provides details on each pair of transducers used for these measurements. The amplitude transmission coefficient was obtained by dividing the amplitude with the Saran present by the amplitude without the Saran present.

The results of these measurements and a fit of the amplitude transmission coefficient given by Equation 1 are shown in Figure 1. The fit parameters correspond to a speed of sound of 2400 m/s and an attenuation coefficient of 5.0 nepers · m^{-1} · MHz$^{-1.5}$ · $f^{1.5}$. The results of this fit for the speed of sound and attenuation coefficient of Saran Wrap were used in Equation 3 to produce a table of transmission coefficients using Equation 3 for each sample that was sent to each participating laboratory over the range of 1 to 50 MHz.

Data Acquisition and Analysis

The laboratory numbers in the following sections have been assigned randomly and do not correspond to the order of institutions listed on the first page of the article.

Table 2. Transducers Used in Measurement of Saran Wrap Amplitude Transmission Coefficient

Freq Used, MHz	Transmitter			Receiver		
	Manufacturer/ Part No.	Center Freq, MHz	Diameter, in	Manufacturer/ Part No.	Center Freq, MHz	Diameter, in
1.0	Aerotech/ Delta PN2797	1.0	1.125	Aerotech/ Delta PN2792	1.0	0.50
2.0	Panametrics/ V306	2.25	0.5	Aerotech/ Delta PN2794-1	2.25	0.25
3, 4	Panametrics/ V382	3.5	0.5	Aerotech/ Delta PN2794-2	3.5	0.25
4, 5, 6	Panametrics/ V309	5.0	0.5	Aerotech/ Delta PN2794-3	5.0	0.25
7, 8	Panametrics/ V320	7.5	0.5	Aerotech/ Delta PN 2794-4	7.0	0.25
9, 10	Panametrics/ V311	10.0	0.5	Krautkramer/ Delta COJWM4	10.0	0.25
15–45	Panametrics/ V356	30.0	0.5	Panametrics V356	30.0	0.5

Laboratory 1

Samples were interrogated in a tank containing distilled water at room temperature. A Panametrics model 5800 pulser/receiver and 3 matched pairs of circular (19.1-mm-diameter) focused transducers were used. The center frequencies were 2.25, 3.5, and 5 MHz, respectively. The focal lengths were 50.8, 50.8, and 38.1 mm. Samples were placed in the focal plane. Received signals were digitized (8 bit, 10 MHz) with a LeCroy model 9310C dual 400-MHz oscilloscope and stored on computer (via a General Purpose Interface Bus) for offline analysis.

To measure sound speed, arrival times of received broadband pulses were measured with and without the sample in the water path. Group velocity, c_g, was computed from

$$c_g = \frac{c_w}{1 + \frac{c_w \Delta t}{d}}, \quad (4)$$

where d is the thickness of the sample (measured with calipers), Δt is the difference in arrival times, and c_w is the temperature-dependent speed of sound in distilled water given by Kaye and Laby[36]:

$$c_w = 1402.9 + 4.835T - 0.047016T^2 + 0.00012725T^3 \text{ m/s}, \quad (5)$$

where T is the temperature in degrees Celsius. Temperature was measured with a digital thermometer and ranged between 21°C and 23°C. Each arrival time was computed as follows. The signal envelope was computed with the use of the Hilbert transform. The arrival time was computed from the maximum in the signal envelope. Using the envelope maximum rather than the leading edge of the pulse or zero crossings minimizes errors in estimates of sound speed due to frequency-dependent attenuation.[37]

A through-transmission method was used to measure attenuation. With 2 opposing coaxially aligned transducers (1 transmitter and 1 receiver), transmitted signals were recorded both with and without the sample in the acoustic path. The attenuation coefficient was estimated by a log

Figure 1. Modulus of the amplitude transmission coefficient for a single layer of Saran Wrap with water on both sides as a function of frequency. Measured values are filled circles, and the solid line represents Equation 1, where a speed of sound of 2400 m/s and an attenuation coefficient of 5.0 nepers · m^{-1} · $MHz^{-1.5}$ · $f^{1.5}$ were used to obtain the best fit to the experiment.

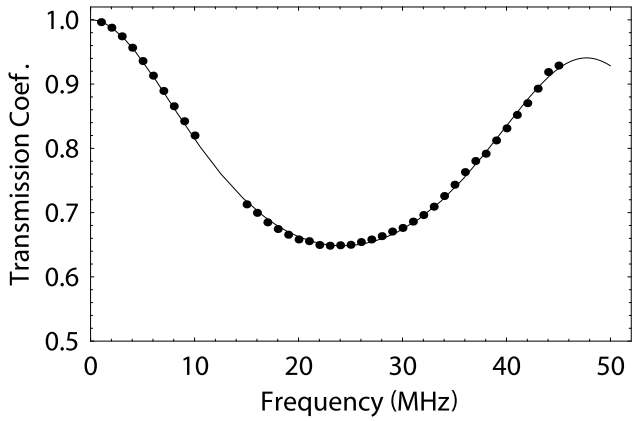

spectral difference technique.[38] Potential diffraction-related errors in this insertion technique may be ignored, provided that the speed of sound in the phantoms is close to that of water.[39]

Backscatter coefficients were measured by a reference phantom method.[28] Approximately 25 echoes were acquired from each phantom by translating the transducer laterally between acquisitions. The front surface of the phantom was aligned with the transducer focal plane. Radio frequency data were gated to isolate the interior of the phantom and to exclude specular echoes. The range gate was 1.8 cm long and began 2 mm beyond the specular echo. The ratios of the squared moduli of the fast Fourier transforms of the test phantom RF data to reference phantom data were computed. Compensation for attenuation was performed with Equation 17 from O'Donnell and Miller.[21]

All measurements were compensated for losses due to transmission through the Saran Wrap layer.

Laboratory 2

All measurements were performed in distilled, highly degassed (Po_2 = 1.3 mg/L) water at 22 ± 0.2°C. All measurements were compensated for the transmission coefficient through the samples' surfaces.

Source transducers were driven by a Panametrics model 5800 pulser/receiver. Three spherically focused transducers were used as sources for measurements of sound speed, attenuation, and backscatter: (1) Panametrics model V380 (diameter of 25.4 mm, center frequency of 3.9 MHz, fractional bandwidth [–3 dB] of 42%, focal length of 90 mm, –6-dB focal beam width of 1.5 mm, and –6-dB depth of focus of 25 mm), (2) Panametrics model V321 (diameter of 19.1 mm, center frequency of 8.4 MHz, fractional bandwidth of 34%, focal length of 95 mm, –6-dB focal beam width of 1.1 mm, and –6-dB depth of focus of 38 mm), and (3) ValpeyFisher Corporation (Hopkinton, MA) model IS1004HR (diameter of 12.7 mm, center frequency of 10 MHz, fractional bandwidth of 42%, focal length of 38 mm, –6-dB focal beam width of 0.8 mm, and –6-dB depth of focus of 25 mm).

The hydrophone used for sound speed and attenuation coefficient measurements was a 1-mm^2 bilaminar membrane hydrophone (model 804; Perceptron, Plymouth Meeting, PA). Sound speed was determined by Equation 4. The reference sound speed for water was taken to be 1488 m/s. Transit time difference (Δt) was measured via a correlation integral technique[40] between the water path and through-tissue signals collected at the hydrophone. Sample thickness was measured with a ruler. The attenuation coefficient was measured by the same log spectral difference method used by laboratory 1.

Backscatter coefficients were estimated by a calibrated pulse-echo technique.[26] The power spectrum was determined for regions of interest (20 wavelengths axially by 5 beam widths laterally) by taking the squared magnitude of the Fourier transform of gated sections from the backscattered time signal. A Hamming window was used to gate the time signals. The effects of the equipment on the power spectrum measurement were factored out by dividing by the reference spectrum from a planar acrylic surface with known reflectivity. Also, the medium's attenuation was compensated for.

Laboratory 3

A Panametrics model 5900PR pulser/receiver was used. Two different single-element Panametrics transducers were used to scan the phantoms. The 3.5-MHz transducer had an aperture of 9.5 mm and a focal length of 42 mm; the 5.0-MHz transducer had an aperture of 9.5 mm and a focal length of 50 mm.

The phantoms were scanned in 10 planes separated by 0.5 mm. Each scan plane consisted of 40 scan lines separated by 0.5 mm. Data were digitized by an Acqiris (Monroe, NY) analog-to-digital board operating at a 50 megasamples (MS)/s sampling rate. Each scan line was digitized with 3400 eight-bit samples. Data were acquired with the transducer focus placed at the front (near) surface of the phantom, that is, at a depth of 0 mm, then at depths of 5, 10, 15, 20, 25, 30, 35, and 40 mm, that is, at the rear (far) surface of the phantom.

The speed of sound was calculated by measuring the phantom thickness and then determining the time between zero-crossing of the RF echo signal at the front (near) and rear (far) surfaces of the phantom. Time was determined by counting the number of samples between the zero-crossings. (At 50 MS/s, the duration of 1 sample is 0.02 microseconds.) The transducer was focused midway into the phantom. Phantom thickness was measured with a mechanical vernier caliper

with a digital readout. The speed of sound was computed as c = 2 * thickness/(0.02 * samples), where the factor of 2 takes into account the round-trip distance for echoes to propagate.

Attenuation was determined by plotting spectral midband values (expressed in decibels relative to reflections from a glass plate) as a function of depth into the phantom. The computations were made for each depth with the focus at the given depth. Midband values were computed for the bandwidth that provided an adequate SNR at all usable focal lengths. Signal-to-noise considerations limited us to 4 depths for phantoms A and C and to 5 depths for phantom B. The sound speed differences between immersion bath water and the phantoms were taken into account in determining the actual focal zone depths, which in all phantoms were closer to the near surface of the phantom than the depths corresponding to transducer displacements of 5, 10, 15, 20, and 25 mm. The average of midband values computed in all planes for each transducer-phantom combination was used to determine the slope of midband as a function of true depth into the tissue. Attenuation, α, was computed as

$$\alpha = \frac{1}{2 f_c} * \left(\frac{\Delta M}{\Delta d} \right), \quad (6)$$

where f_c is the center midband frequency; the factor 2 accounts for the round-trip distance to the actual depth; and $\Delta M/\Delta d$ is the slope of the linear regression of midband versus true depth.

The backscatter coefficient, *BSC*, was computed as

$$BSC = \frac{P_{BS} / P_0}{\Omega * D}, \quad (7)$$

where P_{BS} is the power of signals backscattered from the phantom; P_0 is the power of signals backscattered from a perfect reflector (glass plate); Ω is the solid angle subtended by the transducer; and D is the depth of the insonated volume (0.3969 L, where L is the length of the Hamming window used in these studies). P_{BS}/P_0 is equivalent to the midband value; the relationship is P_{BS}/P_0 = 10 exp (M/10), where M is the normalized or system-corrected midband value (expressed in decibels relative to the reference value).

Laboratory 4

A reference phantom method was applied to measure backscatter and attenuation coefficients using an Acuson 128XP scanner equipped with L7 and V4 array transducers (Siemens Medical Solutions, Mountain View, CA) and modified to provide intermediate frequency data. Echo signals were digitized at 64 MS/s with 8-bit precision.

For sound speed measurements, the transit time from the front interface to the back interface of the cylinder was averaged over 20 nonadjacent beam lines. The thickness of the cylinder was measured with calipers. Sound speed was estimated with the use of the range equation.

A 4-microsecond Blackman-Harris window was modulated by cos ($\omega_o t$) and sin ($\omega_o t$), where ω_o is the analysis frequency, and t is the echo arrival time. Signals from the test cylinders were convolved by each set of quadrature bandpass coefficients, the bandwidth of which was determined by the window duration.[28] The filtered echo signals in each quadrature channel were then squared, and the 2 waveforms were added, producing a single time-dependent waveform. Averaging over all the independent waveforms resulted in an averaged and filtered signal intensity versus depth for each test cylinder at the analysis frequency. The analysis for both transducers was performed in 0.25-MHz steps over the useful bandwidth. The same analysis was applied to the signals from the reference phantom.

Depth-dependent ratios of filtered echo signal intensities from the test cylinders to intensities from the reference phantom then were obtained. The logarithm of the intensity ratio plotted versus depth was quasilinear. The slope of a line fitted to these data was proportional to the difference between the attenuation coefficient of the test cylinder and that of the reference phantom. Because the latter was known, the attenuation in the test cylinder could be deduced. The ratio was compensated for attenuation losses versus depth. The average of this compensated ratio versus depth was multiplied by the backscatter coefficient of the reference phantom to yield the backscatter coefficient for the test cylinder.

Laboratory 5

The experimental setup consisted of a water tank, a Wavetek model 81 function generator, an Amplifier Research model 75A250 RF power

amplifier, a LeCroy model 9410 digital storage oscilloscope, and several pairs of unfocused transducers (Panametrics and KB Aerotech [now GE Inspection Technologies], Lewistown, PA) with various center frequencies. The function generator created a 30-cycle low-amplitude voltage signal, which was amplified and sent to a transmitting transducer. The received signal was displayed on an oscilloscope, which was triggered with a pulse from the function generator that was synchronous with the onset of the output voltage pulse. Received waveforms with and without the sample in the ultrasound path were acquired.

Sound speed was computed from Equation 4 with c_w =1488.4 m/s (22.0°C).[41] Sample thickness was measured with calipers. A zero-crossing was used as a marker for arrival time measurement. Attenuation was measured by a log spectral difference method as discussed in the section for laboratory 1.

The measurement of backscatter coefficients was performed according to the method of Chen et al.[29] Echo signals from broadband source pulses were compared with the echo from a plane reflector. Data were acquired from the sample in a tank of degassed and distilled water. A function generator (FG 5010; Tektronix, Inc, Beaverton, OR) created 1-cycle sinusoidal pulses with a frequency near the transducer center frequency (3.5 MHz). The pulses were amplified with a broadband RF power amplifier (240L; ENI, Rochester, NY) and used to drive the transducer. This resulted in a broad-bandwidth acoustic pulse with approximately 50% fractional bandwidth. Echo signals were received and amplified with a Panametrics 5052UA pulser/receiver. A 10-microsecond interval was digitized at 100 MS/s with a LeCroy 9310A digital storage oscilloscope. Echo signals from the samples were obtained for 98 positions by translating the sample in a raster fashion with the use of a stepper motor system.

Laboratory 6

Transducers with center frequencies of 10 and 15 MHz were built in-house for use in this study. The computer-controlled acoustic field scanning program was used to measure the beam pattern. A calibrated hydrophone, HP function generator (Hewlett-Packard Company, Palo Alto, CA), ZHL-32A amplifier (Mini-Circuits, Brooklyn, New York), TDS-520 oscilloscope (Tektronix, Inc), and DC power supply were used.

The speed of sound and attenuation were measured by a substitution method as described by laboratory 1. The reference speed of sound in water was 1540 m/s. Sample thickness was measured with calipers. A substitution method was used to measure backscatter coefficient[20] (also see laboratory 7 methods). A flat stainless steel block was used for a reference reflector.

Laboratory 7

For sound speed measurements, a Panametrics 5-MHz, 12.7-mm-diameter transducer was used. The Panametrics 5052UA pulse generator was used as a source. A LeCroy 9400A digital oscilloscope was used to digitize RF data.

Samples were placed between the transducer and a steel reflector. The time delays for the echoes from the reflector (T_m) and from both interfaces of the sample (t_1 and t_2) were measured. The sound speed (c_m) was then calculated from

$$c_m = [(T_w - T_m)/(t_2 - t_1) + 1] * c_w, \quad (8)$$

where T_w is the propagation time measured when the sample is removed. The reference speed of sound in water, c_w, was 1481 m/s.[42]

For attenuation and backscatter measurements, a pair of 7.5-MHz, 6-mm-diameter transducers (Echo Ultrasound, Reedsville, PA) was used. The source was a Wavetek 191 function generator. A log spectral difference method (see methods for laboratory 1) was used to compute the attenuation coefficient.

For backscatter measurements, a protection circuit (Expander, DEX-3; Matec, Northborough, MA) consisting of a series of high-frequency diodes was placed between the source and the transducer. Two limiters were placed between the transducer and the oscilloscope. The backscattered signals were digitized by a 500-MS/s analog-to-digital converter (CS 8500; Gage Applied Technologies, Montreal, Quebec, Canada) at a 250-MS/s sampling rate. The specimen was placed at the Rayleigh distance of a nonfocused transducer. The backscatter coefficient in a cylindrical sample volume in the specimen was determined by measuring the backscattered power and normalizing it to the power reflected from a perfect plane reflector (to correct for incident intensity and beam characteristics).[20] Phantom thickness was measured with calipers.

Laboratory 8

The transmitting transducer was excited with a broadband pulse generated by a fast-transition metal oxide semiconductor field effect transistor switch (model PVX-4150; Directed Energy Inc, Fort Collins, CO) under the timing control of a digital delay/pulser (model DG535; Stanford Research Systems, Sunnyvale, CA). The switch was used to hold off a 150-V DC voltage from a power supply (model PS310; Stanford Research Systems). The received signal was conditioned with an amplifier (model BR-640A; Ritec Inc, Warwick, RI) before being captured in a 12-bit digitizer (model CS12100; Gage Applied Technologies) at 100 Ms/s. Each waveform (2048 samples) was a temporal average of 256 acquisitions. The sample was moved in 1-mm steps to collect signals from 225 independent sites in a 15 × 15 grid. All experiments were performed at 22°C.

The speed of sound was measured with a through-transmission method as explained in the methods for laboratory 7. The speed of sound in water was taken to be 1490.8 m/s. A transmitting transducer (5-MHz center frequency, 12.7-mm diameter, and 25.4-mm focus; model A309S-SU; Panametrics) was positioned so that its focus was at the front interface of the phantom sample. A receiving transducer (5-MHz center frequency, 25.4-mm diameter, and 50.8-mm focus; model V307; Panametrics) was placed so that its focus overlapped that of the other transducer.

To measure attenuation, a through-transmission measurement was performed with the sample in place and with the sample removed (water path only). The baseline DC offset of the signals was then subtracted. Signals were isolated with a 5.12-microsecond rectangular window. A log spectral difference method was used (see laboratory 1). Corrections for the transmission coefficient of the sample interfaces were performed.

Backscatter measurements were performed with the same 5-MHz transmitting transducer as above in the pulse-echo mode. The receiving electronics were protected from the exciting pulse by cross-diode protection circuitry (Diplexer RDX-2; Ritec). The focus of the transducer was placed to begin near or slightly after the front wall of the sample. The analysis of the backscattered signal was performed by positioning a 2.56-microsecond Hamming window 3.2 microseconds below the first detected echo from the front wall of the sample. The frequency-dependent power spectra were then calculated for each independent site and then averaged. The resulting mean apparent backscattered power spectrum was then referenced to the signal reflected from the surface of an acrylic plate (amplitude reflection coefficient = 0.37) placed at the focus.[43]

The backscatter coefficient was computed by the formula derived by Chen et al.[30]

$$\eta(f) \cong \frac{\left\langle |V_s(f)|^2 \right\rangle}{|V_{ref}(f)|^2} \frac{r_0^2}{l \cdot \pi a^2 \cdot E_\infty} \exp\left[-(2/\pi)(G_p/\pi)^{-0.5}\right] \cdot F(\alpha,\tau) \cdot \frac{R^2}{T^2 C^2}, \quad (9)$$

where $\langle |V_s(f)|^2 \rangle$ is the ensemble average of backscattered power spectra from medium; $|V_{ref}(f)|^2$ is the backscattered power spectrum from the planar reflector at focus; r_0 is the radius of curvature of transducer; l is the length of the windowed backscatter signal ($c\tau/2$); a is the radius of the active element of the transducer; and $E_\infty = 0.46$. R is the reflection coefficient of the reference surface; T is the intensity transmission coefficient of the water–Saran Wrap–phantom interface; and C is the correction for the windowing function (C = 0.63 for Hamming).[29] The attenuation correction was given by

$$F(\alpha,\tau) = e^{4\alpha x} e^{\alpha c \tau} \frac{2\alpha c \tau}{e^{\alpha c \tau} - e^{-\alpha c \tau}}, \quad (10)$$

where $a(f)$ is frequency-dependent attenuation; x is the length of the material before start of the window; c is the speed of sound in the material; τ is the duration of the windowed backscatter signal.

Measurements of Uniformity and Drift

Measurements of the speed of sound, attenuation coefficients, and backscatter coefficients were made at 22°C in December 2002 and January 2003 on at least 9 phantoms from each of the 3 sets (A–C) before the samples were sent from the University of Wisconsin to the various participants. After the participants had completed their measurements, each participant's 3 phantoms were returned to the University of Wisconsin, where measurements were repeated at 22°C in January and February 2004 according

to the same procedures as those used before the samples had been sent out. Thus, any change (drift) in the material properties of the samples could be assessed. Measurements were performed at multiple frequencies throughout the 2- to 14-MHz range.

Results

In the results that follow, laboratories are anonymously labeled numbers 1 through 8, assigned randomly. The numbers in the figures correspond to the laboratory identification numbers in "Materials and Methods" but do not correspond to the order of the institutions listed on the first page of this article.

Figure 2 shows measurements of attenuation coefficients for the 3 phantoms, as functions of frequency, for the 8 laboratories. Agreement was within 0.15 dB · cm^{-1} · MHz^{-1} for phantom A and within 0.2 dB · cm^{-1} · MHz^{-1} for phantom B but only within 0.5 dB · cm^{-1} · MHz^{-1} for phantom C.

Figure 3 shows measurements of sound speed for the 3 phantoms, as functions of frequency, for the 8 laboratories. There was broad agreement for most laboratories, but some measurements (laboratories 3, 4, and 6) were at times 30 to 60 m/s greater than the majority.

Figure 4 shows measurements of backscatter coefficient for the 3 phantoms, as functions of frequency, for the 8 laboratories. In the case of phantom A (Figure 4A), most measurements showed similar rates of increase of the backscatter coefficient with frequency between 2 and 5 MHz. The laboratories that performed measurements between 5 and 9 MHz seemed to agree that the backscatter coefficient was roughly constant within that frequency range. The solid curve in Figure 4A depicts the theoretical backscatter coefficient, based on the theory of Faran,[44] assuming a scatterer diameter of 82.5 μm (the midpoint of the range from 75 to 90 μm). The theory should not necessarily be taken to be a perfectly accurate estimate because it is based on numerous assumptions and approximations. The beads were not perfect spheres, as the theory assumes, and their true material properties were not known (generic values for glass were used instead). The true scatterer number density was only known to within about 10%. The theory ignores coherent scattering and multiple scattering, which may have been present. The true distribution of scatterer sizes was not known. Nevertheless, it is perhaps worthwhile to point out that laboratory 2 obtained the closest agreement with theory. Laboratories 1, 4, and 8 agreed with theory to within about a factor of 2. Moreover, most laboratories measured frequency dependence of backscatter to be fairly consistent with theoretical prediction.

In the case of phantom B (Figure 4B), very good agreement existed among the laboratories

Figure 2. Measurements of frequency-dependent attenuation coefficients for phantom A, phantom B, and phantom C.

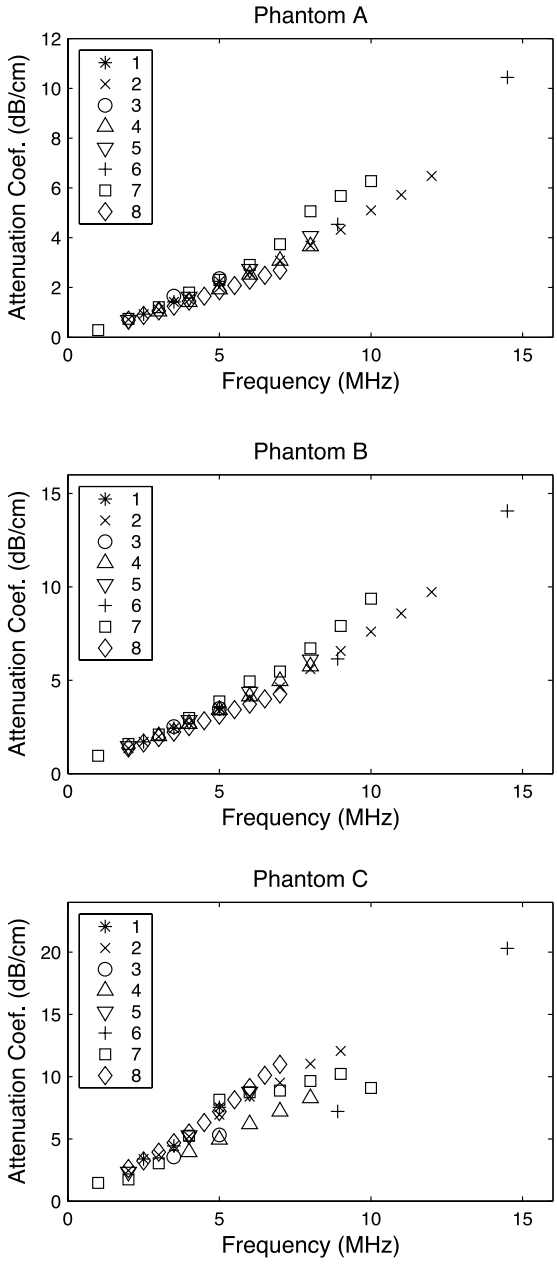

(except laboratory 7) regarding the magnitude and frequency dependence of the backscatter coefficient. The solid curve in Figure 4B depicts the theoretical backscatter coefficient, based on the theory of Faran,[44] assuming a scatterer diameter of 26 μm (the midpoint of the range from 9 to 43 μm). As explained above, caution must be exercised in comparison of experimental data to this theory. The dashed curve in Figure 4B indicates the frequency dependence of backscatter for Rayleigh scattering (frequency to the fourth power), which is valid at frequencies less than 6 MHz. Most laboratories measured frequency dependence of backscatter to be fairly consistent with theoretical prediction.

Figure 3. Measurements of sound speed (SOS) for phantom A, phantom B, and phantom C.

Figure 4. Measurements of frequency-dependent backscatter coefficient for phantom A, phantom B, and phantom C. Solid curves correspond to the theoretical backscatter coefficients, based on the theory of Faran.[44] The dashed curve in B indicates the frequency dependence of backscatter for Rayleigh scattering (frequency to the fourth power), which is valid at low frequencies.

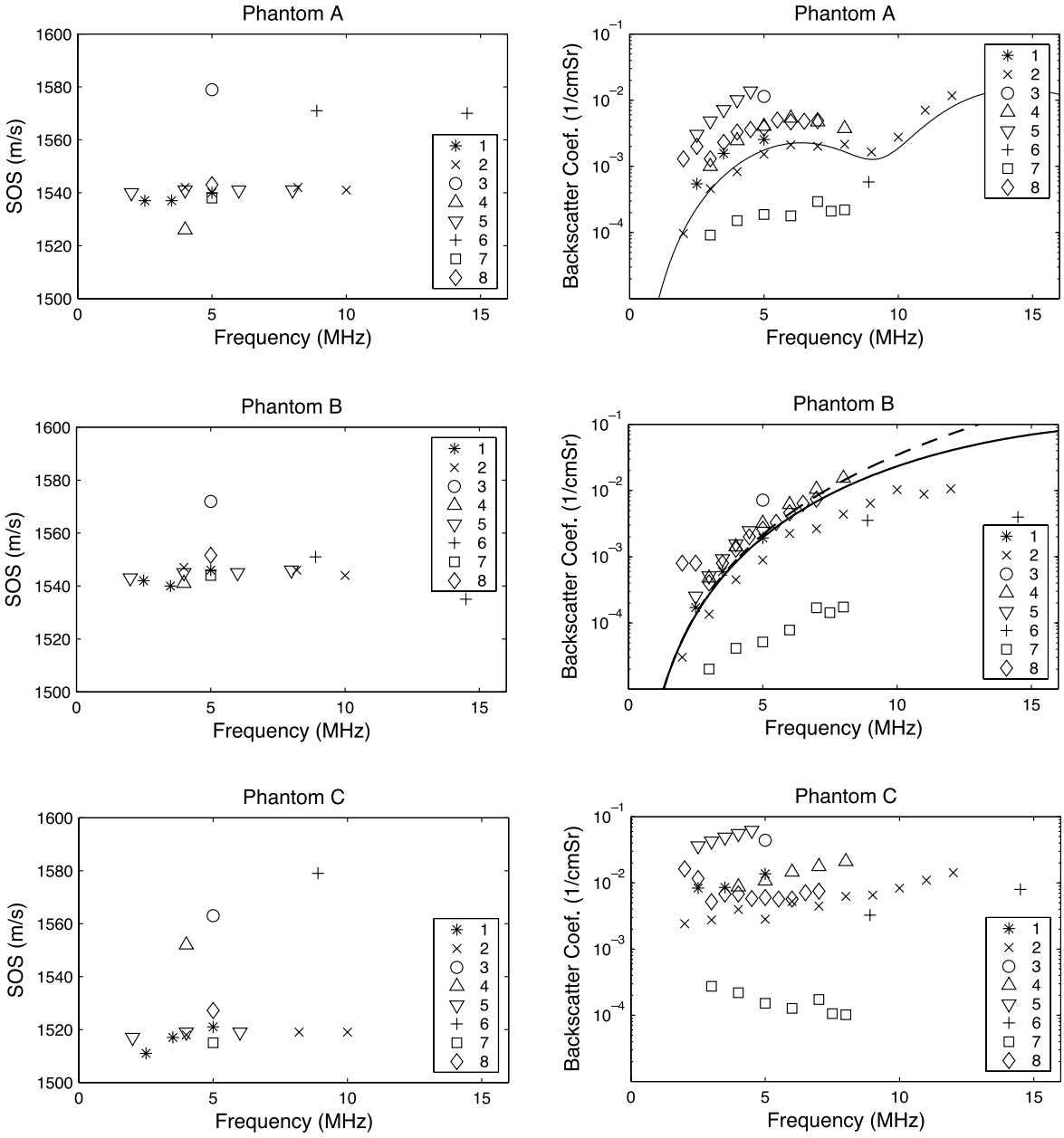

Agreement in backscattering measurements across laboratories was poor for phantom C (Figure 4C). The laboratories generally agreed, however, that the frequency dependence of the backscatter coefficient was much flatter for phantom C than for phantoms A and B. The material properties of the scatterers for phantom C were not known sufficiently well to permit a meaningful theoretical estimate of the backscatter coefficient based on Faran's theory.[44] As in the case for phantom A, the results from laboratories 1, 2, 4, and 8 seemed to cluster together.

Table 3 shows measurements of phantom uniformity. The numbers in the table show within-batch ranges (maxima minus minima) of measurements of sound speed, the attenuation coefficient (at 5 MHz), and the backscatter coefficient (at 5 MHz) performed at the University of Wisconsin before distribution to the participating laboratories. In all cases, the variation in sound speed was no more than about 3 m/s. The variation for the attenuation coefficient (near 5 MHz) was less than 0.1 dB/cm for phantoms A and B and about 0.6 dB/cm for phantom C. The variations for the backscatter coefficient were less than or on the order of 36% for all 3 phantoms.

Table 4 shows changes in measurements of acoustic properties between December 2002 and January 2003 (before samples were sent to participating laboratories) and January 2004 and February 2004 (after samples were returned by participating laboratories) assessed at the University of Wisconsin. In all cases, sound speed drifted by no more than about 2 m/s. The attenuation coefficient at 5 MHz drifted by no more than about 0.1 dB/cm. The backscatter coefficient drifted by no more than 10% for all 3 batches.

Table 3. Phantom Uniformity

Parameter	A	B	C
c, m/s	1.7	2.5	3.2
α, dB/cm	0.06	0.08	0.6
BSC, %	21	30	36

Shown are ranges (maximum minus minimum) for within-batch measurements of sound speed (*c*), attenuation coefficient (α, at 5 MHz), and backscatter coefficient (BSC, at 5 MHz) for phantom batches A, B, and C. The backscatter coefficient range is expressed as a percentage of the average backscatter coefficient for the batch. Values for attenuation and backscatter coefficients were obtained from power law fits to measured data.

Discussion

The range of variation of the absolute magnitude of backscatter coefficient measurements was about 1 (excluding laboratory 7) or 2 (including laboratory 7) orders of magnitude. There was better agreement among laboratories regarding measurements of the frequency dependence of backscatter, which is an indicator of scatterer size. For example, when scatterers were small compared with the ultrasonic wavelength, experimental frequency-dependent backscatter coefficient data obtained by the participating laboratories were usually consistent with the expected Rayleigh scattering behavior (proportional to frequency to the fourth power).

Sound speed variations (whether due to phantom nonuniformity, temporal drift, or disparity of measurements among participating laboratories) observed in this study are not likely to explain a substantial fraction of the disparity in backscatter coefficient measurements. The effect of errors (or variations of any sort) of sound speed estimates on backscatter coefficient estimates is as follows. Errors in sound speed measurement lead to inaccurate range gating of backscattered signals. For a gate duration Δt, the corresponding gate length from a pulse-echo signal is $d = c\Delta t/2$. A relative error in sound speed ε_c ($|c_{meas} - c_{true}|/c_{true}$) would correspond to the same relative error in estimated gate length ε_d ($|d_{meas} - d_{true}|/d_{true}$) and scattering volume ε_v. (Scattering volume is proportional to the product of gate length and beam width.) The computed backscatter coefficient is inversely proportional to the assumed scattering volume. Therefore, the relative error in the backscatter coefficient would be $\varepsilon_{BSC} = \varepsilon_v = \varepsilon_d = \varepsilon_c$. From Figures 2–4, it can be

Table 4. Phantom Drift

Parameter	A	B	C
c, m/s	–0.1	1.1	1.5
α, dB/cm	0.03	0.01	0.11
BSC, %	<2	<10	<5

Shown are average changes in measurements of parameters between January 2003 (before distribution to participating laboratories) and January 2004 (after participating laboratories performed measurements) for phantom batches A, B, and C. The maximum minus minimum backscatter coefficient (BSC) is expressed as a percentage of the average backscatter coefficient for the batch. Values for attenuation (α) and backscatter coefficients were obtained from power law fits to measured data; *c* indicates sound speed.

seen that in the worst case (phantom C), measurements varied by as much as about 70 m/s or about 5%. This is a high variability for a relatively easy measurement. However, it would only produce 5% variations in backscatter coefficient measurements, a negligible fraction of the total observed (1–2 orders of magnitude). The within-batch nonuniformity (Table 3) and temporal drift (Table 4) of sound speed of the phantoms were less than or on the order of 3 m/s, again corresponding to negligible variations of backscatter coefficient estimates.

It is also unlikely that attenuation coefficient variations (whether due to phantom nonuniformity, temporal drift, or disparity of measurements among participating laboratories) observed in this study could explain a significant fraction of the disparity in backscatter coefficient measurements. Errors in attenuation coefficient estimates lead to inaccurate compensation of backscatter data for the effects of attenuation. If attenuation coefficient variation were a primary determinant of backscatter coefficient variation, then those laboratories underestimating attenuation coefficients would be expected to undercompensate their backscatter data and report low backscatter coefficients. Similarly, those laboratories overestimating attenuation coefficients would be expected to report high backscatter coefficients. Thus, one might expect a positive correlation between estimates of attenuation and backscatter coefficients. However, as indicated in Figure 5, no such positive correlation was observed in this study. In addition, the within-batch nonuniformity (Table 3) and temporal drift (Table 4) of attenuation coefficients for the phantoms were less than or on the order of 0.6 dB/cm at 5 MHz. Because the phantoms were about 4 cm thick, this would lead to a range of attenuation of less than or on the order of 1.5 dB at 5 MHz. This is far too small to produce anywhere near the 1 or 2 order(s) of magnitude (ie, 10–20 dB) variation in the backscatter coefficient estimate that was observed.

Within-batch nonuniformity and temporal drift of backscatter coefficients were less than 36%. Again, this variability is small compared with the 1 to 2 orders of magnitude variation of measurements reported by the participating laboratories.

One possible source of disparity that remains is that different data reduction algorithms, even if implemented correctly, may yield substantially different values. Some methods use focused transducers, whereas others use unfocused transducers. Under some conditions, focused and unfocused transducers may yield disparate results.[45] For calibration, some methods use a planar reflector, whereas others use a phantom that contains distributed pointlike scatterers. The model for the backscattering object may be

Figure 5. Scatterplots of attenuation coefficient measurements versus backscatter coefficient measurements at 5 MHz for phantom A, phantom B, and phantom C.

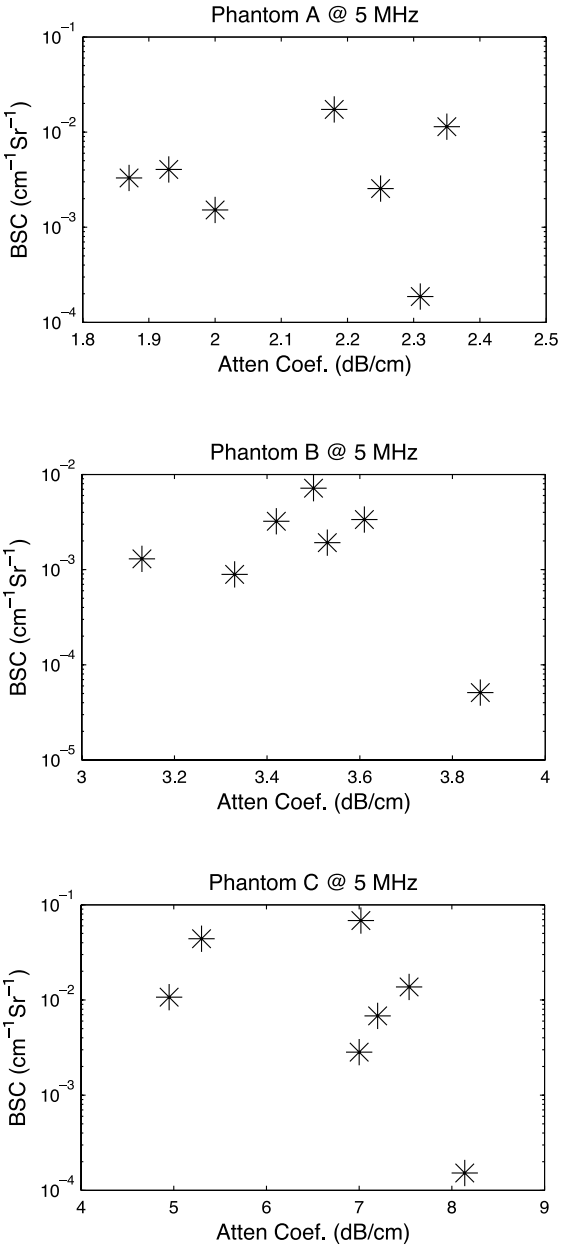

continuous or discrete. Under these circumstances, production of different quantitative values by different approaches should not be surprising.

Experimental error may also be an appreciable source of disparity. Data acquisition issues (correct positioning of transducers relative to samples, correct positioning of reference reflectors, avoidance of saturation of receiving electronics and digitizer, and optimization of transmitted power to maximize the SNR without saturation) could contribute to errors. In addition, data reduction software errors, which may remain undetected in the absence of a reference standard test, can also exacerbate inaccuracy. For example, although laboratories 6 and 7 both used the same method for backscatter coefficient estimation, they obtained markedly dissimilar results for phantoms B and C. At least one of these laboratories is likely to have had experimental or software error.

Although considerable disparity existed among the participating laboratories regarding absolute levels of backscatter, the level of agreement regarding frequency dependence of the backscatter coefficient was fair. This establishes some promise for standardized estimation of scatterer size.

Finally, the present study offers several improvements over the previous AIUM-sponsored interlaboratory comparison.[19] First, the upper range of frequencies has been extended from 7 to 9 MHz (the highest frequency for which multiple measurements are available for comparison). Second, the analysis of phantom uniformity and drift has been expanded from attenuation and sound speed (in the previous study) to also include backscatter (in this study). Consequently, the candidate mechanisms for disparity in backscatter coefficient measurements in this study could be narrowed down more convincingly to algorithmic differences and software/experimental error. Third, the results in this study were compared with theoretically expected backscatter coefficients, allowing independent and objective evaluation of laboratory measurements. Fourth, and most important, the test phantoms in this study (unlike the previous study) have been returned to those laboratories requesting them. Now participating laboratories have standardized test objects, with properties documented in this article (with moderate consistency if not complete unambiguity), to help them refine their backscatter coefficient measurement methods. It is hoped this will lead to improved consistency in future reports of frequency-dependent backscatter coefficients among the participating laboratories.

References

1. Shung KK, Sigelmann RA, Reid JM. Scattering of ultrasound by blood. IEEE Trans Biomed Eng 1976; 23:460–467.
2. Angelsen BAJ. A theoretical study of the scattering of ultrasound from blood. IEEE Trans Biomed Eng 1980; 27:61–67.
3. Madaras EI, Barzilai B, Perez JE, Sobel BE, Miller JG. Changes in myocardial backscatter throughout the cardiac cycle. Ultrason Imaging 1983; 5:229–239.
4. Campbell JA, Waag RC. Measurements of calf liver ultrasonic differential and total scattering cross sections. J Acoust Soc Am 1984; 75:603–611.
5. Lizzi FL, King DL, Rorke MC, et al. Comparison of theoretical scattering results and ultrasonic data from clinical liver examinations, Ultrasound Med Biol 1988; 14:377–385.
6. Wear KA, Milunski MR, Wickline SA, Perez JE, Sobel BE, Miller JG. Differentiation between acutely ischemic myocardium and zones of completed infarction in dogs on the basis of frequency-dependent backscatter. J Acoust Soc Am 1989; 85: 2634–2641.
7. Turnbull DH, Wilson SR, Hine AL, Foster FS. Ultrasonic characterization of selected renal tissues. Ultrasound Med Biol 1989; 15:241–253.
8. Insana MF, Hall TJ, Fishback JL. Identifying acoustic scattering sources in normal renal parenchyma from the anisotropy in acoustic properties. Ultrasound Med Biol 1991; 17:613–626.
9. Insana MF, Wood JG, Hall TJ. Identifying acoustic scattering sources in normal renal parenchyma in vivo by varying arterial and ureteral pressures. Ultrasound Med Biol 1992; 18:587–599.
10. Sehgal CM. Quantitative relationship between tissue composition and scattering of ultrasound. J Acoust Soc Am 1993; 94:1944–1952.
11. Wear KA, Garra BS, Hall TJ. Measurements of ultrasonic backscatter coefficients in human liver and kidney in vivo. J Acoust Soc Am 1995; 98:1852–1857.

12. Feleppa EJ, Kalisz A, Sokil-Melgar JB, et al. Typing of prostate tissue by ultrasonic spectrum analysis. IEEE Trans Ultrason Ferroelectr Freq Control 1996; 43:609–619.

13. Silverman RH, Folberg R, Boldt HC, et al. Correlation of ultrasound parameter imaging with microcirculatory patterns in uveal melanomas. Ultrasound Med Biol 1997; 23:573–581.

14. Russell MD, Sun H, Wicks ML, et al. Ultrasonic nondestructive evaluation applied to prostate cancer detection. Nondestr Test Eval 1998; 14:237–256.

15. Wear KA. Frequency dependence of ultrasonic backscatter from human trabecular bone: theory and experiment. J Acoust Soc Am 1999; 106: 3659–3664.

16. Hall CS, Scott MJ, Lanza GM, et al. The extracellular matrix is an important source of ultrasound backscatter from myocardium. J Acoust Soc Am 2000; 107:612–619.

17. Oelze ML, Zachary JF, O'Brien WD Jr. Characterization of tissue microstructure using ultrasonic backscatter: theory and technique for optimization using a Gaussian form factor. J Acoust Soc Am 2002; 112:1202–1211.

18. Oelze ML, O'Brien WD, Blue JP, Zachary JF. Differentiation and characterization of rat mammary fibroadenomas and 4T1 mouse carcinomas using quantitative ultrasound imaging. IEEE Trans Med Imaging 2004; 23:764–771.

19. Madsen EL, Dong F, Frank GR, et al. Interlaboratory comparison of ultrasonic backscatter, attenuation, and speed measurements. J Ultrasound Med 1999; 18:615–631.

20. Sigelmann RA, Reid JM. Analysis and measurement of ultrasound backscattering from an ensemble of scatterers excited by sine-wave bursts. J Acoust Soc Am 1973; 53:1351–1355.

21. O'Donnell M, Miller JG. Quantitative broadband ultrasonic backscatter: an approach to nondestructive evaluation in acoustically inhomogeneous materials. J Appl Phys 1981; 52:1056–1065.

22. Nicholas D, Hill CR, Nassiri DK. Evaluation of backscattering coefficients for excised human tissues: principles and techniques. Ultrasound Med Biol 1982; 8:7–15.

23. Lizzi FL, Greenebaum M, Feleppa EJ, et al. Theoretical framework for spectrum analysis in ultrasonic tissue characterization. J Acoust Soc Am 1983; 73:1366–1373.

24. Campbell JA, Waag RC. Normalization of ultrasonic scattering measurements to obtain average differential scattering cross sections for tissues. J Acoust Soc Am 1983; 74:393–399.

25. Madsen EL, Insana MF, Zagzebski JA. Method of data reduction for accurate determination of acoustic backscatter coefficients. J Acoust Soc Am 1984; 76:913–923.

26. Insana MF, Hall TJ. Parametric ultrasound imaging from backscatter coefficient measurements: image formation and interpretation. Ultrason Imaging 1990; 12:245–267.

27. Yao LZ, Zagzebski JA, Madsen EL. Backscatter coefficient measurements using a reference phantom to extract depth-dependent instrumentation factors. Ultrason Imaging 1990; 12:58–70.

28. Zagzebski JA, Yao LX, Boote EJ, Lu ZF. Quantitative backscatter imaging. In: Shung KK, Thieme GA (eds). Ultrasonic Scattering in Biological Tissues. Boca Raton, FL: CRC Press Inc; 1993:451–486.

29. Chen JF, Zagzebski JA, Madsen EL. Tests of backscatter coefficient measurement using broadband pulses. IEEE Trans Ultrason Ferroelectr Freq Control 1993; 40:603–607.

30. Chen X, Phillips D, Schwarz KQ, Mottley JG, Parker KJ. The measurement of backscatter coefficient from a broadband pulse-echo system: a new formulation. IEEE Trans Ultrason Ferroelectr Freq Control 1997; 44:515–525.

31. Madsen EL, Frank GR, Dong F. Liquid or solid ultrasonically tissue-mimicking materials with very low scatter. Ultrasound Med Biol 1998; 24:535–542.

32. Chin RB, Madsen EL, Zagzebski JA, Jadvar H, Wu X-K, Frank GR. A reusable perfusion supporting tissue-mimicking material for ultrasound hyperthermia phantoms. Med Phys 1990; 17:380–390.

33. D'Astous FT, Foster FS. Frequency dependence of ultrasonic attenuation and backscatter in breast tissue. Ultrasound Med Biol 1986; 12:795–808.

34. Madsen EL, Zagzebski JA, Frank GR. Oil-in-gelatin dispersions for use as ultrasonically tissue-mimicking materials. Ultrasound Med Biol 1982; 8:277–287.

35. Ford RD. Introduction to Acoustics. Amsterdam, the Netherlands: Elsevier; 1970:77.

36. Kaye GWC, Laby TH. Table of Physical and Chemical Constants. London, England: Longman; 1973.

37. Ragozzino M. Analysis of the error in measurement of ultrasound speed in tissue due to waveform deformation by frequency-dependent attenuation. Ultrasonics 1981; 19:135–138.

38. Kuc R, Schwartz M. Estimating the acoustic attenuation coefficient slope for liver from reflected ultrasound signals. IEEE Trans Son Ultrason 1979; 26: 353–362.

39. Xu W, Kaufman JJ. Diffraction correction methods for insertion ultrasound attenuation estimation. IEEE Trans Biomed Eng 1993; 40:563–570.

40. Devries P. Computational Physics. New York, NY: John Wiley & Sons; 1994.

41. Marczak W. Water as a standard in the measurement of speed of sound in liquids. J Acoust Soc Am 1997; 102:2776–2779.

42. Dunn F, Edmonds PD, Fry WJ. Absorption and dispersion of ultrasound in biological media. In: Schwan HP (ed). Biological Engineering. New York, NY: McGraw-Hill; 1969:205–332.

43. Selfridge A. Approximate material properties in isotropic materials. IEEE Trans Son Ultrason 1985; 32:381–394.

44. Faran JJ. Sound scattering by solid cylinders and spheres. J Acoust Soc Am 1951; 23:405–418.

45. Yuan YW, Shung KK. The effect of focusing on ultrasonic backscatter measurements. Ultrason Imaging 1986; 8:121–130.